The physics of plasma etching

1991 Phys. Scr. 1991 299

(http://iopscience.iop.org/1402-4896/1991/T35/058)

Physica Scripta. Vol. T35, 299–308, 1991.

The Physics of Plasma Etching

J. I. Ulacia F. and S. Schwarzl

Siemens AG, ZFE SPT, Otto-Hahn-Ring 6, D-8000 Munich 83, Germany

Received March 21, 1990; accepted December 30, 1990

Abstract

Today, plasma etching is the most important patterning technique in the manufacture of semiconductor integrated circuits; however, the physics and chemistry involved in this process are still not well understood. This paper describes the most important physical processes that control this technique and explains their individual governing equations. In practice, the solution of the complete set of plasma equations has many limitations because the physical-dimension domains for every process varies from the atomic scale to typical reactor dimensions (10^{-9}–10^{0} m). For simplicity, the problem is separated into five independent categories as – gas kinetics, electrodynamics, transport of ions and neutrals, surface kinetics, and time evolution. In this modular format, it is possible to study each physical process in detail and to include more-or-less details in individual models depending on the characteristics of each etching environment. Examples of different etching processes are described where the contribution of individual etching mechanisms are important.

1. Introduction

Characteristic for the rapid progress in semiconductor-circuit manufacture is the continuous miniaturization of devices with submicron dimensions as a result of the rapidly growing integration density and device complexity. Highly significant for the manufacturing process are lithographic techniques for the generation of patterns in photomasks and dry-etching techniques for the transfer into the substrate. Plasma etching prevails over wet-chemical etching mainly because of its anisotropic pattern transfer capabilities below 2.5 μm. In spite of the remarkable process results, this technique remains highly empirical and much experience and intuition are necessary to compensate the limited understanding of the numerous physical and chemical phenomena associated with this process.

The practical requirements are growing with new IC generations due to smaller feature size, higher complexity, rising topography, and design innovations like trench memory cells or multilevel metallization schemes. Very demanding is the simultaneous fulfilling of the various requirements which are

- high anisotropy for a high-fidelity pattern transfer from the photomask into the underlayer with minimum features approaching 0.3 μm for 64 M DRAMs.
- the realization of 3D structures with aspect ratios higher than 10 : 1.
- highly selective and residue-free etching of conventional, new materials, and layered combinations.
- low processing temperatures ($\leqslant 120$°C) to prevent dimensional variations of organic masks.
- avoidance of radiation damage and contamination.
- qualification for production, i.e. high reproducibility, low particle generation, high up-time and high throughput.

Many times these requirements are of conflicting nature and several trade-offs must be established, for example between anisotropy and selectivity. In addition, multi-step processing is often inevitable. Modified etching characteristics are also necessary for additional applications such as sidewall tapering to relax topography, etch back planarization to fill contact holes, vias and small spaces, blanket-film removal from the wafer front and back, and post-etching treatments to remove contamination or damage introduced by certain processes.

Development is further complicated by the close interaction of different steps within the overall process sequence, which consists of more than 350 single steps for 4 M DRAMs. Etching is strongly influenced both by properties of the film to be etched and by the photoresist mask which affects subsequent processes and device performance; for example oxide quality, contact-hole resistance, and reliability of metalization lines. In addition, there are long learning cycles caused by full or partial process runs necessary to determine the effect of specific modifications in one step of the final electrical behaviour of the device.

In relation to the plasma-surface interaction, plasma etching may range from pure physical sputtering based on momentum transfer between energetic ions and the surface, to physical and chemical processes where ions, electrons, photons and reactive neutrals play important roles during the process. Improved results can be obtained by combining the advantages of these mechanisms to overcome the disadvantages of pure sputtering and pure chemical etching.

The plasmas used in this process are partially ionized gases (degree of ionization $\leqslant 10^{-4}$) that are ignited and maintained by electrical a.c.-fields in pressures of typically 10^{-2}–10^{3} Pa (10^{-4}–10^{1} Torr) and serve as sources of reactive neutrals and ions consumed in the process. Energy gained by charged particles is transmitted to neutrals by elastic and inelastic collisions that generate reactive species. Charged particles and reactive neutrals are eliminated from the system by several mechanisms as charged-species recombination, molecular polymerization, surface recombination at the chamber walls, chemical reaction at the wafer surface, and through the pumping system.

The striking variety of different plasma etching systems and gas mixtures used in modern IC development and manufacturing lines is certainly a consequence of the different requirement for various process applications. Usually, these specifications cannot be met by universal etching systems, or gas chemistries, and probably this situation is also a reflection of the insufficient scientific insight into the complex and diverse nature of the process.

Some of the difficulties detailed above are the result of the different dimensional domains found in the system. When we simulate the gas kinetics and electric fields we work in dimensions of meters, while when working with ion transport

across the sheath it is in the millimeter regime, for the surface kinetics it is on the atomic scale, and the time evolution of a typical structure is in the micron regime. Therefore the models needed to analyze the plasma etching process must be different depending on the dimension we want to study.

This paper does not present an exhaustive review on the different topics related to plasma etching, but rather gives an idea on the different problems and directions on which the area has expanded.

2. Plasma etching in a modular approach

To enhance the understanding of the etching process and to simplify the equations that describe the environment, the study can be separated into modules or blocks that concentrate on specific subproblems. As illustrated in Fig. 1 the plasma process can be separated into five different groups [1] as – Electrodynamics, Gas Kinetics, Transport, Surface Kinetics, and Time Evolution. Even though the first three blocks are closely related and share many of their governing equations, they have been segmented according to the emphasis they have on a particular problem; nevertheless, conceptually they should be attacked globally in a coherent approach.

The electrodynamics module concentrates on the calculation of the potentials, electric fields, currents, and concentrations of charged particles in the gas phase. As boundary conditions, it requires data on the geometry of the reactor, the potentials applied to the electrodes, generation and recombination rates of charged particles, and energy balances. In plasma conditions this problem is highly non-linear because of the high diffusivity of electrons for Poisson's equation.

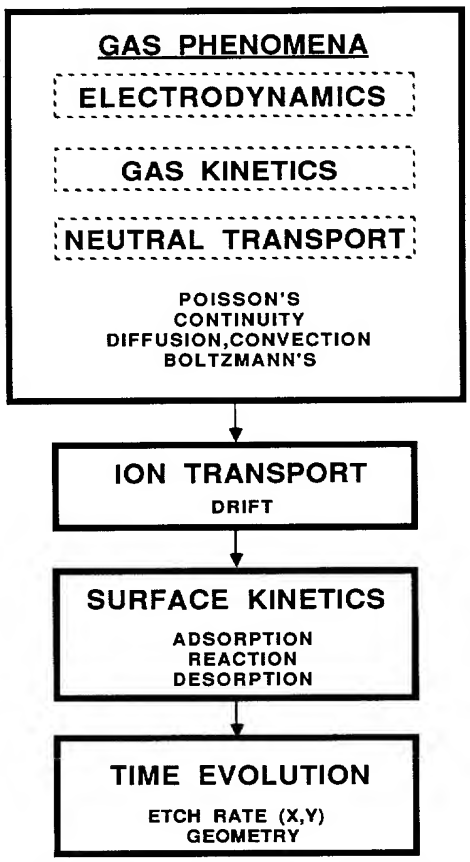

Fig. 1. Modular representation of the plasma process. Each independent problem has been isolated in one block to facilitate its study.

The gas kinetics module determines the particle generation and loss in the plasma by processes such as dissociation, recombination, attachment, and ionization. This module is computed either by the solution of the Boltzmann transport equation when the collision-cross sections are known, or by the solution of the coupled generation and loss equations once experimental or theoretical reaction rate constants are available. Many of these rates are a function of the electron density and temperature obtained by the electrodynamics module.

When considering the transport module, a separation between the ions and the neutrals must be made because charged particles respond to electric fields which are strong near the wafer surface while neutral particles respond only to concentration gradients. In addition, positive ions acquire large amounts of energy ($E_i \approx 500\,\text{eV}$) at the sheath boundary and transfer it to the surface having high reactivities. Neutrals, on the other hand, have concentrations four orders of magnitude higher than positive ions but low energies (near room-temperature $E_n \approx 0.03\,\text{eV}$) and as a result low reactivities. The independent study of these contributions has specific applications. For example, when the ion component is responsible for the desorption of surface molecules, the technique is called sputtering, and the neutral component through the creation of volatile by-products with reactions is chemical etching. In general, ion bombardment produces directional etching while the neutrals contribute to isotropic etching. The understanding of plasma technique becomes conceptually difficult when both mechanisms influence the outcome of the trench profile as will be explained later.

At the atomic scale, surface kinetics takes into account the etching contribution of all the reactive particles that arrive on the silicon wafer. For a reaction to proceed, three main steps are necessary – adsorption of reactive particles, chemical reaction to form a volatile by-product, and desorption of the by-product. In addition, two secondary processes play a significant role because they accelerate or retard the overall reaction rate. The first enhances the etch rate by ion bombardment while the second reduces it by the deposition of inhibitor layers that mask the surface.

The time evolution module computes the time-dependent modification of the structure being patterned at the micron regime. During the etch-patterning of a device, the instantaneous fluxes of particles that arrive on the surface depend on the wafer topology, the specific step to be performed, the materials used, and the evolution time at which the process is carried out. This problem affects the final structure of the device because shadowing and reflections modify the fluxes of particles along the surface as a function of time; therefore, the time development of the structure must be analyzed to determine the final structure dimensions.

It is known that in a process that depends on different sequential steps, the overall throughput is determined by the slowest or "rate-limiting step". This knowledge can be applied to plasma etching technique because it is a sequential processes; (*a*) the electric potentials applied to the electrodes generate electric fields that accelerate free electrons, (*b*) these electrons collide with neutral particles and produce ions and

reactive radicals, (*c*) the ions are accelerated in the sheath boundary and deposit energy to the wafer surface, (*d*) the neutrals are transported from the bulk of the plasma to the surface, (*e*) here, they react to generate volatile by-products, (*f*) the by-products desorb into the gas phase and are carried away by the pumping system. Therefore, in the plasma environment when one of the steps controls the overall process it is not necessary to compute all the physical and chemical equations, but rather the ones that correspond to the bottle-neck step. Many processes are limited by only one of these mechanisms and their analysis is greatly simplified, as will be illustrated; however, for some etching process there is no particular rate limiting step and the process operates in a combined regime. As a result, the main problem in the process description is the identification of the rate limiting steps in a specific reactor environment (with particular geometry, power conditions, etching gases, wafer materials, pressure and temperature).

3. Gas phenomena

For perspective, gas phenomena refers to all the processes that take place in the gas phase – electrodynamics, gas kinetics, and transport of neutrals and ions. This section provides an overview of the governing equations and focuses on their interactions; later each subtopic will be studied independently.

In a general format, the equations that describe this domain are Poisson's, mass-, chemical-species-, momentum-, and energy-continuity equations as

$$\nabla^2 V = \frac{q}{\varepsilon_0}\left(\sum_{i=1}^{n} N_i^+ - \sum_{j=1}^{m} N_j^- - N_e\right) \tag{1}$$

$$\frac{\partial \rho}{\partial t} + \nabla \cdot (\rho \boldsymbol{u}) = 0 \tag{2}$$

$$\frac{\partial}{\partial t}(\rho m_i) + \nabla \cdot (\rho \boldsymbol{u} m_i) = \nabla \cdot (D_i \nabla m_i) + G_i \tag{3}$$

$$\frac{\partial}{\partial t}(\rho u) + \nabla \cdot (\rho \boldsymbol{u} u) = \nabla \cdot (\mu_m \nabla u) - \frac{\partial P}{\partial X_i} + B + v \tag{4}$$

$$\frac{\partial}{\partial t}(\rho H) + \nabla \cdot (\rho \boldsymbol{u} H) = \nabla \cdot (\kappa_m \nabla T) + S_h \tag{5}$$

where V is electrostatic potential, q is electron charge, ε_0 is permittivity of free space, N_i^+ is concentration of positive ions, N_j^- is concentration of negative ions, N_e is electron concentration, ρ is the density of the media, t is time, $\boldsymbol{u}$ is the velocity vector, m_i is mass fraction of the particle 'i', D_i is diffusion coefficient, G_i is the generation term in the bulk, μ_m is viscosity of the mixture, P is pressure, B is the body force per unit volume (i.e., buoyancy or Lorentz forces), v represents viscous terms in addition to those expressed by μ_m, H is specific enthalpy that is related to the temperature through heat capacity C_p as $dH = C_p\, dT$, κ_m is thermal conductivity of the mixture, T is temperature, and S_h is the volumetric rate of heat generation. The ideal gas law $P = \rho RT$ closes the equation set and must be included to describe the variations of density along the reactor.

The equations for conservation of chemical species (3), momentum (4), and energy (5) consider the effect of both convection and diffusion. It should be noted that for momentum continuity there is one equation for every coordinate solved, for particle continuity one equation for every particle in the plasma, and for energy continuity one equation for every particle with a different temperature distribution.

In solving this set of equations (eqs. (1–5)) it is possible to obtain the self-consistent spatial distribution of potential, electric field, concentration of all different species, pressure, temperature distributions for particles, generation and loss rates, and the fluxes of particles including electric currents. However, the solution of this problem is, within itself, a difficult task and a subdivision must be made to study different phenomena independently.

4. Electrodynamics

This section deals with the electrical characteristics of the gas consisting of Poisson's equation (eq. (1)), and the particle continuity for charged particles (eq. (3)), with or without the energy balance equation for electrons (eq. (5)). The neutral gas molecules are assumed to be in thermal equilibrium with the reactor wall.

Several authors have attempted to solve this problem making different assumptions. For example, Graves and Jensen [2] considered a small system of one ion-type and electrons and solved the time dependent Poisson's, particle-continuity for both species and the energy balance equation for electrons (eqs. (1, 3, 5)). The results obtained include the d.c. and r.f. distributions of potential, electric field, ion and electron concentrations, ionization rates, current densities, and energy losses in one dimension. From their r.f. results the concentration of charged particles in the bulk follows an ambipolar diffusion profile, the plasma is driven by large displacement currents, and there is a large gas ionization peak near the power electrode where secondary emission was activated.

Barnes and collaborators [3] study the same equations applied to an argon discharge and include Townsend's first ionization coefficients. The calculation of the transport and ionization coefficients as a function of electric field were performed via Monte Carlo techniques to determine mobilities and diffusivities. These simulations are used to determine the effects of unequal area electrodes, illustrating that larger particle fluxes can be obtained when the area ratio is varied. In this work the electron density in the plasma does not follow the ambipolar diffusion, but contains two peaks near the sheaths.

In the same direction, Boeuf [4] included in one dimension – one positive ion, one negative ion and electrons, with Poisson's equation, momentum and particle balances for each particle. The local-field approximation was used as in the previous simulations to simplify the computation. The spatial distributions of particles follow the ambipolar diffusion model except that negative ions have a strong effect on the shape of the distribution. For the time-dependent simulation for sheath currents, the results agree with the ones obtained from circuit model simulations [5]. More recently the same author [6] extended his work on 2D simulation results with the same assumptions, but neglecting negative ions.

Even though these results are very valuable for the description of the gas phase phenomena, the solution is highly computation intensive and requires the use of supercomputers.

In addition, because the electric field varies drastically near the electrode surfaces and the mean free path has the same order of magnitude as the sheath thickness, the local field approximation and the fluid dynamic model is questionable in this region. Therefore, a better description for ion transport in the sheath boundary is necessary and obtained from Monte Carlo methods.

With many simplifying assumptions and based on plasma-impedance experimental data, several authors have followed a simpler approach called the circuit model [5, 7] to compute electron density, sheath thickness, and ion current in the sheath. In this technique, the electrical characteristics of the plasma are represented by an electrical net of passive and active devices, where each circuit element represents one current transport mechanism. The experimental variables required for this analysis are the peak a.c. voltage $V_{a.c.}$, the d.c. bias voltage $V_{d.c.}$, the peak a.c. current $I_{a.c.}$ and the phase angle between the a.c. signals θ. Because this method is based on experimental data its advantages are on the general application to all plasma processing conditions (even with many gases), fast computation, and direct interpretation of important current transport mechanisms through the direct analogy of circuit elements. This is done even when complex gas interactions are found and the cross sections are unknown. The main disadvantages are the lack of theoretical support for the different circuit interconnects and the lack of self-consistent computation for all the variables that control the process.

5. Gas kinetics

The computation of the term G_i in eq. (3) is the main subject of gas kinetics because even for very simple etching environments there is a large amount of particles and reaction-rate equations. This problem can be solved through the Boltzmann transport equation when the electron–collision cross sections are known, or by a model that incorporates the reaction rate constants for the different reactions when these data are available.

The first approach analyses the ways in which a particle gains or looses energy in a differential volume (in seven dimensions — 3 spatial, 3 velocities, and time). A particle can migrate to another coordinate by means of its inherent velocity, it can gain or loose energy from electric or magnetic fields, or can collide with another particle and exchange energy. These mechanisms are represented by the Boltzmann transport equation as

$$\frac{\partial \mathscr{F}}{\partial t} + \boldsymbol{u} \cdot \nabla \mathscr{F} + \frac{\boldsymbol{F}}{m_j} \cdot \frac{\partial \mathscr{F}}{\partial \boldsymbol{u}} = \left(\frac{\partial \mathscr{F}}{\partial t}\right)_{coll} \tag{6}$$

where $\mathscr{F}$ is the particle distribution function, the last term represents all the collision phenomena in which this distribution is affected, and $\boldsymbol{F}$ represents external forces. For charged particles $\boldsymbol{F}$ is the Lorentz force as

$$\boldsymbol{F} = -q(\boldsymbol{E} + \boldsymbol{u} \times \boldsymbol{B}) \tag{7}$$

where E and B are electric and magnetic fields respectively. As can be imagined, this equation must be solved for every particle in the discharge and the solution is not trivial.

For an SF_6 environment, Kline [8] computed the electron kinetics assuming the reaction to be dissociative. Using both a Monte Carlo code and solving the Boltzmann transport equation eighteen reactions are postulated. The electrical characteristics of a chlorine plasma have been studied by Rogoff and collaborators [9]. Here, the plasma bulk is considered to be volume-controlled where electron balance is dominated by single-step electron-inpact ionization and attachment, and the electron-distribution function is in equilibrium with the instantaneous electric field. In the r.f. cycle, it is observed that ionization takes place where the E/n ratio is high and attachment where the current-densities are small. The calculated time-averaged power input per unit length is in agreement with experimental values.

The second approach is based on the solution of the rate equations once sufficient kinetic data are known either from experimental data or form theoretical studies. This process is much simpler than the previous because it is only necessary to include all the rate equations for which data exist in the source term G_i. If the reaction is heterogeneous on the surface, then the reaction rate should not be included in G_i but as a boundary condition to the continuity equation.

Plumb and Ryan [10] studied the gas phase reactions of CF_4 with O_2 and identified 49 different chemical reactions in the gas phase with determined and assumed reaction-rate constants. Later they demonstrated that only 18 of these reactions are important for the correct description of the plasma and the others could be neglected. As can be observed, the variety and reactivity of chemical species in a plasma environment is large and the determination of the rate coefficients is difficult.

6. Transport of radicals

The transport of neutral radicals is obtained when appropriate surface kinetics are applied as boundary conditions in eq. (3) for the species that contribute to etching. For the low pressures used, particle diffusion is sometimes more important than convection and the later can be eliminated from the computation.

The analysis must consider the mass transport and surface kinetics limiting regimes of operation. These limitations appear when there is a sequential transport and surface reaction of a reactive radical A on the surface to form the by-product B.

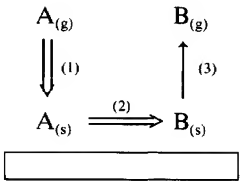

The mass transport limitation is the result of the inability to effectively diffuse species A from the plasma bulk to the surface and depends on the relative magnitude of its diffusion coefficient. The flux of particles J_t is then described by

$$J_t = -D_A \nabla A \tag{8}$$

where D_A is diffusion coefficient of species A in the mixture and ∇A is the concentration gradient. The surface kinetic limitation appears when the transport is efficient and the chemical reaction at the interface is slow. This mechanism is

usually represented by an Arrhenius equation of the form

$$J_k = k_0 \exp(-E_a/kT)A^n \quad (9)$$

where k_0 is a constant, E_a is the activation energy for the kinetic process, k is Boltzmann's constant, T is temperature, and n is a value that determines the order of the chemical kinetics. Under steady state conditions both fluxes should be equal and it is possible to compute the rate as

$$\frac{1}{J_e} = \frac{1}{J_t} + \frac{1}{J_k} \quad (10)$$

where the slowest mechanisms control the reaction.

This analysis is useful to determine macroscopic variables as the overall uniformity of the etching. For example, Economou and collaborators [11] studied the 2D etching uniformity in a parallel plate reactor using a fluid-dynamic approach for an oxygen plasma. They used argon actinometry to quantify the amount of oxygen consumed at the interphase and correlated their results with wafer uniformity data. Their simulations predict the "bull's-eye" found in processed wafers and through scaling parameters give alternative process conditions for reduced non-uniformities.

For an isothermal system in the mass-transfer limited regime, the solution of eqs. (2)–(4) have been successfully computed for the etching of aluminum in a chlorine plasma [12]. In this environment it is possible to neglect the electrodynamics and gas-kinetics parts as a result of the following experimental observations:

- Aluminum is etched by both atomic and molecular chlorine once the native oxide layer has been removed.
- The etch rate is strongly load dependent — higher values for small loads and lower rates for high loads.
- The etch rate is nearly independent of bias voltage — the physics in the plasma do not affect the etching characteristics of the wafers.
- The flow of chlorine that enters the reactor is smaller than the flow of aluminium tri-chloride ($AlCl_3$) that desorbs from the wafer surface — indicating that the desorbing species should have lower ratio of chlorine to aluminum ($AlCl_b$).

Under these conditions, the plasma is necessary to (a) generate all the reactive radicals required in the reaction, (b) maintain an aluminum-oxide free surface by ion bombardment, and (c) keep fast-surface kinetics with the energy deposited by the ions.

The results obtained include the determination of the pressure, velocity and concentration of the chemical species in the reactor with the self consistent computation of etch rates for different reactor loads, and non-uniformity. The good agreement between the simulations and the experimental results is evident in the comparison of non-uniformity of one wafer in a 6 wafer load illustrated in Fig. 2. These simulations are of extreme importance for reactor optimization, not only in plasma etching but in CVD, RPT, and diffusion furnaces.

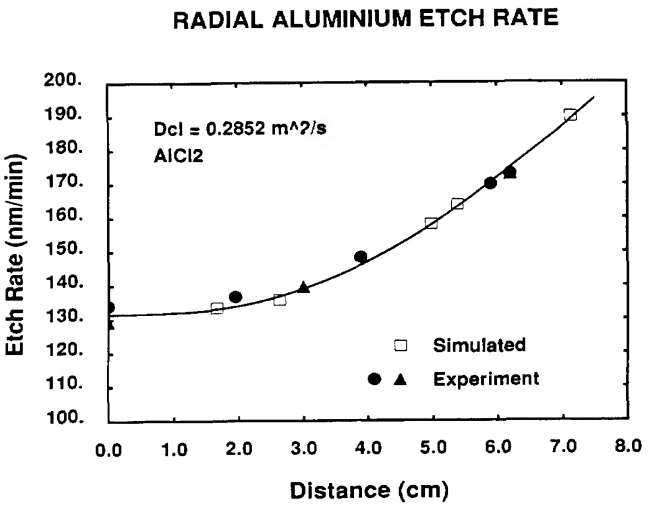

Fig. 2. Experimental and simulated radial wafer uniformities for a 6 wafer batch. The etch rate is largest in the periphery where chlorine side diffusion is large, increasing the etch rate.

7. Ion transport in the sheath

As mentioned previously, the transport of ions in the sheath boundary cannot be computed through fluid-mechanic methods because the sheath-thickness is similar to the mean-free path and the field changes significantly in this region. In these circumstances we cannot assume the gas to be in local thermodynamic equilibrium and the individual trajectories of the ions must be computed to obtain the energy deposited on the surface through the angular-distribution function of ions. Monte Carlo methods [13–15] are ideal for this problem because they analyse the ion transport at different intervals during the ion's flight and include collisions. For example, the program Q-MOCADIF 3D [15, 16] computes the 3D trajectory of different ions across a plasma sheath with many different models for ion-generation distance x (constant, random, or secondary emission), sheath potential V_{sh} (constant, capacitive approx., or resistive approx.), electric field $E(x, t)$ (constant, linear, Child–Langmuir collisionless, Child–Langmuir collision dominated), sheath thickness $l_{sh}(t)$ (constant or sinusoidal). It also includes models for hard and soft collisions including collision-charge transfer. The information used as boundary conditions is obtained by either experimental results or self-consistent simulations described in the electrodynamics section. Figure 3 illustrates two angular-dependent distribution functions for a sheath-thickness to mean-free-path ratio of 1.0 and 3.7 used to compute the etching of silicon with SF_6. This figure also illustrates that ions with the largest energy arrive at the surface without any collisions and with an angle perpendicular to the surface, while the ones that suffer collisions arrive at larger angles with smaller energies.

8. Surface kinetics

The surface kinetics concentrates on the determination of the reaction constants at the atomic scale based on either *ab-initio* computations or on effective sticking coefficients determined from experimental data.

In the first approach, the reactivities of the different particles are determined from first principles. A quantum-mechanical model is proposed that describes the vibrational, rotational and electronic structure of the atoms and computes the possible paths for reaction of these molecules. One disadvantage from this method is the detailed description of each atom that reduces the scope of simulation to

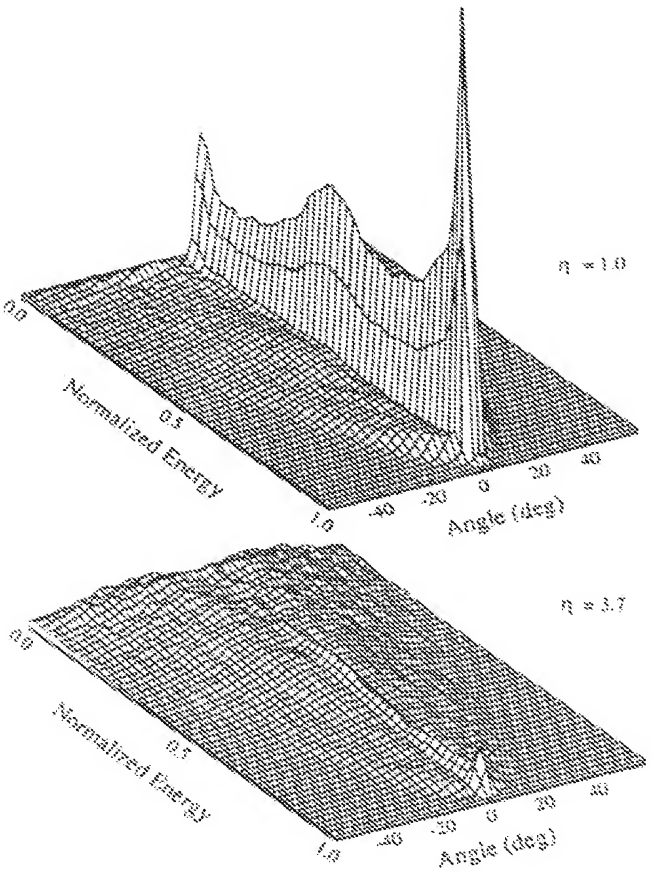

Fig. 3. Monte Carlo angular-ion distribution function for SF_5^+ ions in an SF_6 plasma for two different sheath-thickness to mean-free-path ratios η.

small molecules or clusters. Hartree–Fock calculations provide information of energetic states using descriptions of Molecular-Orbital theory. For example, based on *ab-initio* principles, Seel and Bagus [17] calculated energy as a function of distance of a fluorine atom that approaches a "silicon-like" cluster of adatoms. In the calculation, they used Hartree–Fock wave functions to describe the valence orbitals of both species. The binding energy for F on Si was determined to be a minimum of 3.2 eV at a distance of 1.7 Å, and the barrier height for penetration was on the order of ≈ 1 eV. Comparison with XPS data led to the conclusion that intermediate-surface species form before SiF_4 desorbs.

The second approach uses Monte Carlo methods [1] to determine the joint contribution on the formation of reaction intermediates using effective sticking coefficients. Conceptually, the visualization of this method is simpler because the atoms are represented by solid objects and the reaction probabilities represent macroscopic reaction rate constants. The sticking coefficient is a number from 0–1 that represent the probability of reaction of a chemical species with its collision partner; when it is close to 1 the reaction probability is large. Each collision process has a specific sticking coefficient and the trajectory of each particle is computed as a random walk process.

9. Time evolution

The time evolution module utilizes information described in the previous sections and computes the etch profile progression with time. Here, only the geometrical effects of a structure are analyzed and the etch rates are the result of the local flux of neutrals and ions on the surface as a function of space and time.

The flux of reactive neutrals is determined by diffusion and contributes to the isotropic etch component, while the flux of ions is determined by the plasma conditions and is responsible for the anisotropic etch component. Possible mechanisms for the anisotropy discussed in the literature are chemically-enhanced physical sputtering [18], surface damage generation [19], chemical sputtering [20], direct reactive ion etching [21], activation by surface heating, and ion-assisted desorption.

The isotropic and anisotropic etch rate components are assumed to be proportional to the local flux of neutrals and ion-energy, respectively, and to the angle dependent etch yield, subject to energetic thresholds. The accessibility of ions and neutrals is different for structures with high aspect ratios changing the etch characteristics. Shadowing reduces the ion-energy flux for deep-lying surface points (i.e., in the bottom of a trench or hole) and effectively reduces the anisotropic component. Specular reflection of ions with large incident angles increases the ion flux at the bottom of the trench, near the sidewall, producing higher etch rates known as trenching.

Further effects on the time evolution are caused by physical erosion and faceting of the etching mask leading to a mask widening, crystallographic orientation of single-crystalline material, formation of inhibitor layers by redeposition of material from the mask, polymerization of species from the gas phase, and by stable materials with low sputtering yields.

10. Experimental data

In the previous sections plasma etching has been treated in distinctive modules to isolate the main contributions to the etching phenomena. Here experimental data will be provided that isolate every mechanism detailed above and provide a frame of reference based on this technique.

The phenomena related to electrodynamics and gas kinetics are fundamental for all plasma etch applications and must be addressed by the choice of the etching tool and etching gases. But, for most applications there is one specific and dominating aspect which is decisive for the etching mechanism.

Deep 3-D structures, such as holes and long grooves are required to produce buried storage capacitors for DRAMS or deep isolations for bipolar devices. For both applications trenches between 5 to 10 μm with aspect ratios up to 10 : 1, and vertical to slightly-positive-tapered sidewalls must be obtained. In addition, sidewalls must be smooth and the bottoms flat or rounded depending on the storage cell used. Deep trenches require ion-assisted etching processes with high etch rates and high anisotropy. To avoid undercutting chlorine- or bromine-based plasmas are preferred due to their low spontaneous but high ion-assisted chemical reactivities [22]. The importance of the ion-transport phenomena for deep trench etching with chlorine chemistry is illustrated in Figs. 4–5. The first shows typical profile imperfections occurring in a BCl_3/Cl_2 process in RIE batch systems. Decisive for the ion bombardment are the d.c.-bias voltage and the pressure ranging from -250 to -400 V, and 15 to 20 mTorr

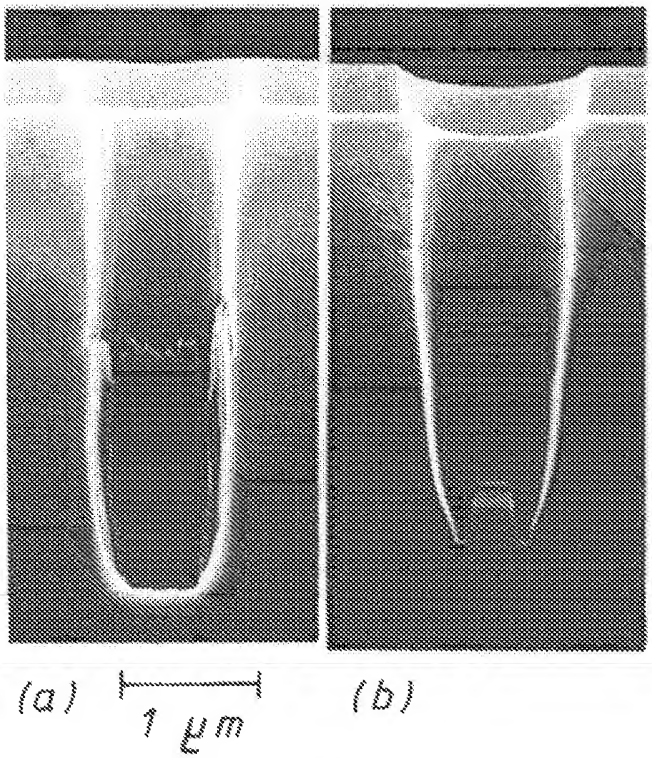

Fig. 4. Profile imperfections occurring during RIE of deep trenches under different process conditions: (a) −275 V d.c. bias, 20 mTorr, (b) −375 V d.c. bias, 15 mTorr.

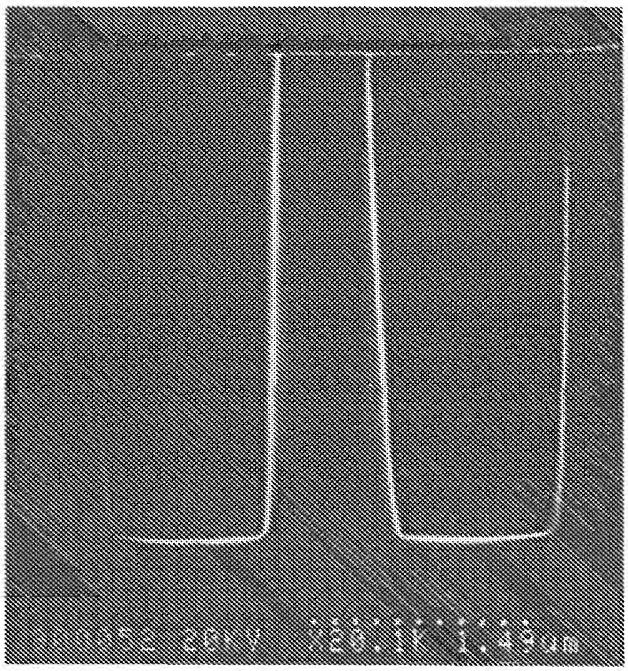

Fig. 5. Deep trenches with ideal profiles etched in a magnetically confined triode system under pure Cl_2 as etching gas (3.7 μm deep, 1.33 μm diameter).

respectively. At lower ion energies with a wider ion-angular distribution function (−275 V, 20 mTorr) step-like irregularities arise at the widewalls, which are correlated to the formation of B_xCl_y inhibitor layers [23]. These layers are removed in the upper region by oblique ions that arrive at the surface at large angles. As a result, silicon is attacked in the upper part leaving behind the residue where the reaction cannot proceed.

Higher ion energies with a narrower ion-angular distribution function (−375 V, 15 mTorr) produce straight sidewalls and spike-like structures at the trench bottom. Less sidewall bombardment by higher ion collimation prevents sidewall film removal and a smoother sidewall; however, the specular reflection of ions with high energy from the sidewalls produced enhanced etch rates at the bottom edge of the trench.

In spite of the systematic parameter variation, it is difficult to produce reproducible profile results with both smooth sidewalls and rounded bottoms simply by ion bombardment. The addition of polymer-forming gases (e.g., CF_3Br [24]) is necessary to improve the profiles under these conditions. Low-energetic and highly collimated ion bombardment produces ideal trench profiles (Fig. 5) when a magnetically confined dual-frequency triode etcher is used with pure chlorine gas, at low pressures (2 mTorr), and with a 100 kHz r.f. power of 50 W [26]. Under these conditions none of the above profile irregularities are found as a result of the low-ion energy and narrow ion-angular distribution functions [25].

The gas kinetics effects can be identified in an SF_6 process [15] where only the gas chemistry was modified, as illustrated in Fig. 6. All the experiments where performed at 13.56 MHz, 0.324 W/cm^2 at 100 mTorr in the same parallel-plate diode reactor and using the same wafer-types to simplify data analysis and reduce external interactions. The first SEM represents the process with pure SF_6 and an SiO_2 mask where large concentrations of atomic fluorine are found producing isotropic profiles. When additives that generate inhibitor layers are included in the reactor, the profile becomes more directional as illustrated in the second SEM where C_2ClF_5 was added as the polymer precursor; again, the mask was SiO_2. Photoresist further increases the generation of inhibitor layers that are effectively deposited on the sidewall of the trench being etched, as illustrated on the third SEM etched with C_2ClF_5 and photoresist mask; here, the profile is completely anisotropic. As it is observed, the trench profiles change dramatically, from fully isotropic to fully anisotropic, according to specific chemistry in the gas phase when all the other parameters are kept constant. The computer simulation for these processes is found underneath each figure.

Regarding the surface-kinetics processes, the specific interactions between reactive species and the material to be etched have a strong impact. For example, chlorine atoms have a very low chemical reactivity with respect to undoped or boron-doped silicon; however, there is a high spontaneous etching component for highly phosphorus- or arsenic-doped silicon [27] that produce undercutting if the sidewalls are not protected by passivation layers. This difference in surface reactivity yields different etching results as illustrated in Fig. 7. An anodically coupled single-wafer plasma etcher with 13.56 MHz r.f. power source can be successfully used for etching both undoped and n^+-doped poly silicon (poly) in a Cl_2/He plasma at 500 mTorr. Anisotropic profiles of undoped poly can be easily obtained using a photoresist etching mask as shown in Fig. 7(a). A line-width gain (0.15–0.2 μm and tapered sidewalls are the consequences of a polymer built-up at the sidewalls originating from the organic

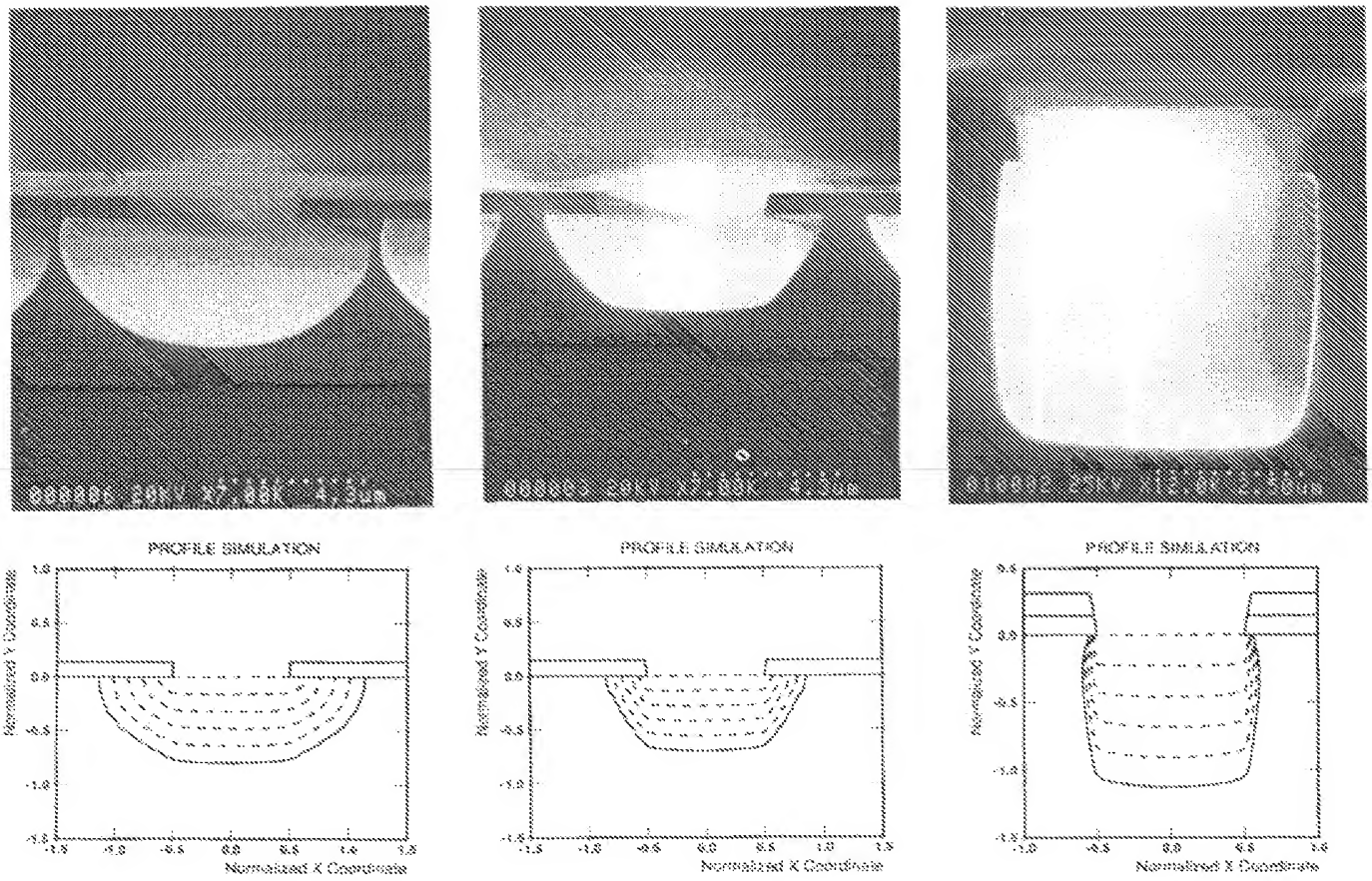

Fig. 6. Effect of the gas chemistry on the etching characteristics of pure silicon in SF_6 plasmas at 0.324 w cm^2 and 100 mTorr. (a) SF_6 100 sccm, SiO_2 mask, (b) SF_6: C_2ClF_5 100 : 100 sccm, SiO_2 mask, (c) SF_6: C_6ClF_5 100 : 100 sccm, photoresist mask.

mask material removed from an etching process with a selectivity of about 1 : 1 between undoped poly and photoresist. Undercutting and spontaneous etching of undoped poly have never been observed.

Much more sensitive is anisotropic etching of highly phosphorus-doped n^+-poly under otherwise identical process conditions. Vertical sidewalls based on inhibitor layers are possible in a narrow process window. Process instabilities may produce insufficient sidewall passivation and sometimes severe undercutting as illustrated in Fig. 7(b). The reasons for such failures are higher selectivity to photoresist as a result of higher n^+-poly etch rate with thinner passivation films, excessive overetch time (> 100%) for high topography, process instabilities caused by oxygen and moisture in the chamber, and insufficient preconditioning. Remedies for the anisotropy problem are the use of species with low inherent surface reactivities (i.e., bromine based) and modern low-pressure etching techniques (i.e., magnetically enhanced RIE and ECR).

The effects of time evolution are evident in deep silicon trenches used for DRAM-storage capacitors etched in a single-wafer dual-frequency triode system using CF_3Br/N_2 gas mixture and CVD-SiO_2 as etch mask material [28]. In this system the plasma density and ion energy are somewhat independently determined by a 13.56 MHz and 100 kHz r.f. power source. The trenches of 4 to 5 μm depth and 1 × 1 μm^2 cross section have almost perfect profiles for DRAM storage capacitors etched at a total gas pressure of 500 mTorr. With increasing aspect ratio, both the depth and the sidewall taper of the trenches are reduced as illustrated in Fig. 8. All the profiles can be explained by flux limitations of ions and neutral species by shadowing. In the center of the large mask windows (100 × 500 μm^2) the etch rate is maximum as a result of an unlimited ion bombardment; in smaller windows (3 × 30 μm^2) the etch rate is sequentially reduced as the aspect ratio increases and is more evident in smaller struc-

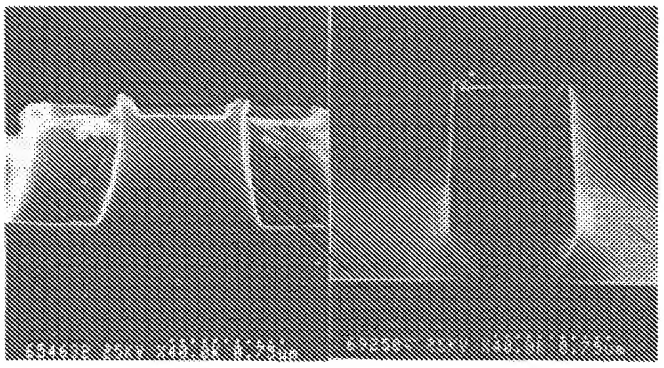

Fig. 7. Profile of a 0.4 μm thick poly etched in a single-wafer parallel plate plasma etcher using Cl_2/He at 500 mTorr; the etching mask is still in place. (a) Undoped poly, (b) highly phosphorus-doped poly.

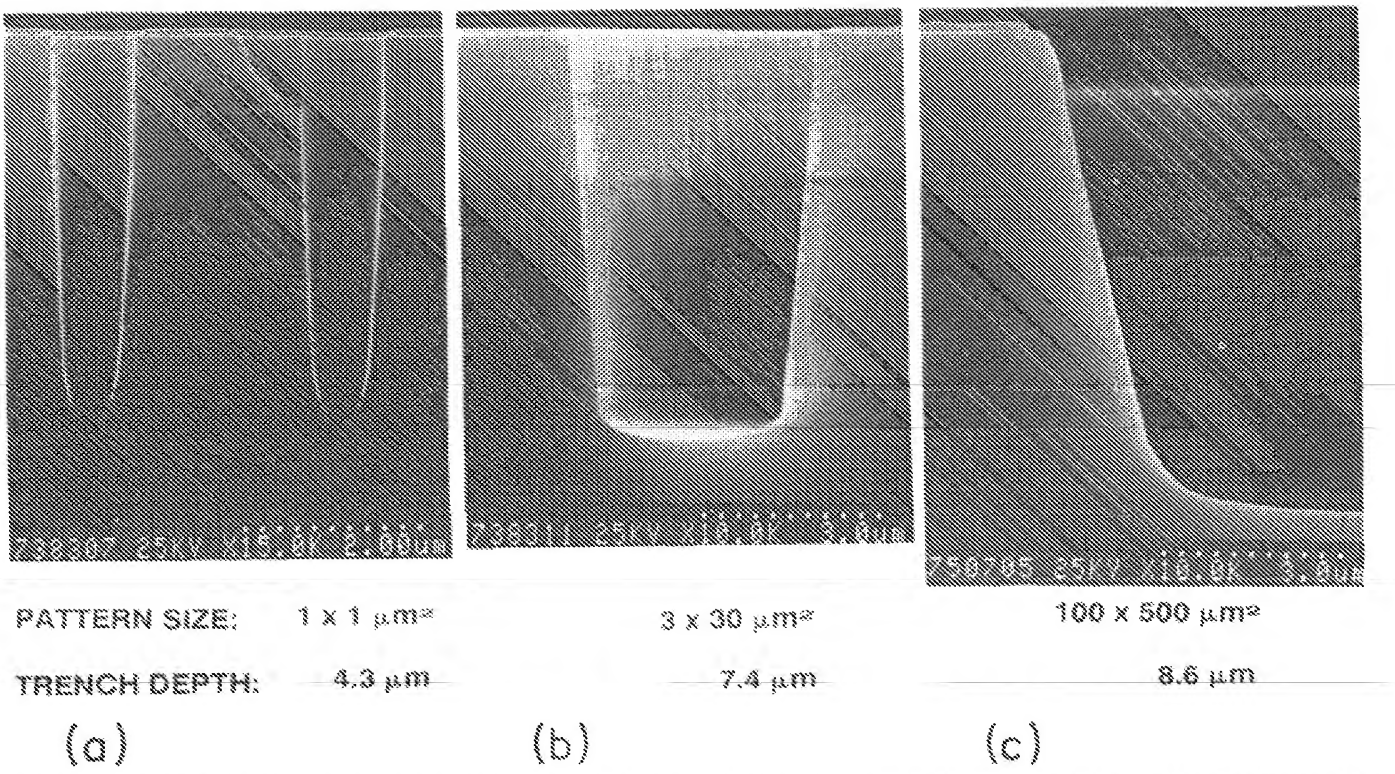

Fig. 8. Pattern size effects of trench etching in a single-wafer dual-frequency triode system using CF_6Br/N_2. The sidewall deposits have been removed by wet chemical cleaning after plasma etching.

tures. When the reaction at the surface is fast and the process operates near the mass-transfer limited regime, shadowing is more effective for neutrals than for ions because they arrive with an isotropic distribution in contrast with the narrow distribution function of the ions.

11. Conclusion

The physical principles of plasma etching are known today, but many difficulties remain both in theoretical, numerical, and practical respects as a result of the complex nature of the topic. The separation of the problem into five categories proved to be a useful concept to study the details characteristic of every phenomenon and isolates the main features found at each simulation domain. This work gives a framework on which more comprehensive models can be implemented and provides a general methodology on which any plasma environment can be studied. As illustrated in this paper, work has expanded in many directions and the primary areas of study have been identified; however, a complete simulation model that incorporates all the mechanisms found in a plasma environment has not been compiled. Further progress in the understanding of physical and chemical plasma and surface phenomena is necessary to support efficiently equipment and process development for microelectronic patterning applications.

Acknowledgements

We would like to thank Dr J. P. McVittie and Dr K. Saraswat of Stanford University and M. Engelhardt, A. Strohbach and J. Berthold of Siemens for providing SEMs and technical data on different processes, and for interesting discussions.

References

1. Ulacia F. J. I., "Theoretical and experimental considerations necessary to build a dry etching process simulator", Technical report G-833-1, Stanford University, Stanford, CA (1988).
2. Graves, D. B. and Jensen, K. F., IEEE Trans. Plasma Physics **PS-14**, 78 (1986).
3. Barnes, M. S., Colter, T. J. and Elta, M. E., J. Appl. Phys. **61**, 81 (1987).
4. Boeuf, J. P., Phys. Rev. **36**, 2782 (1987).
5. Ulacia F. J. I. and McVittie, J. P., Mat. Res. Soc. Symp. Proc. **98**, 203 (1987).
6. Boeuf, J. P., J. Appl. Phys. **63**, 1342 (1988).
7. Ilic, D. C., Rev. Sci. Instrum. **52**, 1542 (1981).
8. Kline, L. E., IEEE Trans. Plasma Physics **PS-14**, 145 (1986).
9. Rogoff, G. L., Kramer, J. M. and Piejak, R. B., IEEE Trans. Plasma Physics **PS-14**, 103 (1986).
10. Plumb, I. C. and Ryan, K. R., Plasma Chemistry and Plasma Processing **6**, 205 (1986).
11. Economou, D. J., Park, S. and Williams, G. D., J. Electrochem. Soc. **136**, 188 (1989).
12. Ulacia, F. J. I. and Berthold, J., submitted to J. Electrochem. Soc.
13. Kushner, M. J., J. Appl. Phys. **58**, 4024 (1985).
14. Thompson, B. E., Sawin, H. H. and Fisher, D. A., J. Appl. Phys. **63**, 2241 (1988).
15. Ulacia, F. J. I. and McVittie, J. P., J. Appl. Phys. **65**, 1491 (1989).
16. Q-MOCADIF-3D Users Manual (Qualtec Inc., P.O. Box. 21-050, Mexico DF, 04000, Mexico, 1990).
17. Seel, M. and Bagus, P. S., Phys. Rev. **B23**, 23 (1981).
18. Mauer, J. L., Logan, J. S., Zichuski, L. B. and Schwartz, G. S., J. Vac. Sci. Technol. **15**, 1734 (1978).
19. Coburn, J. W. and Winters, H. F., J. Appl. Phys. **50**, 3189 (1979).
20. Tu, Y. Y., Chuang, T. J. and Winters, H. F., Phys. Rev. **B23**, 823 (1981).
21. Steinbrüchel, C., Lehmann, H. W. and Frick, K., J. Electrochem. Soc. **132**, 180 (1979).
22. Tachi, S. and Okudaira, S., J. Vac. Sci. Technol. **B4**, 459 (1986).
23. Rangelow, I. W., Thoren, P., Masseli, K., Kassing, R., Engelhardt, M. and Schwarzl, S., Microelectronic Engineering **5**, 387 (1986).

24. Engelhardt, M. and Schwarzl, S., Proc. Symp. on Dry Process, ECS Proc. **88-7**, 48 (1988).
25. Norris, P. and Krogh, O., Proc. 9th ISPC, Pugnochiuso, Italy, page 645 (1989).
26. Engelhardt, M., 2nd Tegal Europe Plasma Seminar, Zürich, page 56 (1990).
27. Mogab, C. J. and Levinstein, H. J., J. Vac. Sci. Technol. **17**, 721 (1980); Okano, H., Yoriike, Y. and Sekine, M., Jap. J. Appl. Phys. **24**, 68 (1985).
28. Engelhardt, M. and Schwarzl, S., Proc. 2nd Int. Symp. on ULSI Sci. Tech., May 1989, ECS Proc. **89-9**, 505 (1989).